Measurement 61 (2015) 192–205

Contents lists available at ScienceDirect

Measurement

journal homepage: www.elsevier.com/locate/measurement

Exquisite CCD camera design for an optical computed tomography scanner

Wen-Tzeng Huang [a], Chao-Nan Hung [b], Sun-Yen Tan [b], Chiu-Ching Tuan [b], Chin-Hsing Chen [c], Wen-Tsai Sung [d,*]

[a] Minghsing University of Science and Technology, Department of Computer Science, Taiwan, ROC
[b] National Taipei University of Technology, Graduate Institute of Computer and Communication Engineering, Taiwan, ROC
[c] Central Taiwan University of Science and Technology, Department of Management Information Systems, Taiwan, ROC
[d] National Chin-Yi University of Technology, Department of Electrical Engineering, Taiwan, ROC

ARTICLE INFO

Article history:
Received 13 April 2014
Received in revised form 18 September 2014
Accepted 23 September 2014
Available online 6 October 2014

Keywords:
OCT
CCD
Spatial resolution
MTF
Random noise
Flat-field correction

ABSTRACT

The OCT (Optical Computed Tomography) in order to obtain the precise dose distribution relies on high accuracy (low noise) and high spatial resolution of the image capture system. Therefore, this study proposes a high-resolution CCD-based camera systems design. Part of the low noise, we propose a variety of CCD signal processing to eliminate noise, such as bias clamp, random noise and pixel response non-uniformity. According to the experiment results, our CCD signal processing algorithm can guarantee low noise output. At exposure time of 150 ms, the coefficient of variation of the pixel is reduced from 12.37% to 0.51% by flat-field correction, in the same measurement standards, our system SNR (30.12 dB) better than other brand CCD camera (25.31 dB) and other brand CMOS camera (29.53 dB). Part of the high spatial resolution, we propose high-performance camera design (optical lens, image sensor, image processing) to ensure high spatial resolution output. In MTF50 (Modulation Transfer Function 50%), our camera (1024 × 1024) get the 745 LW/PH (Line Width/Picture Height), close to 73% of the limited resolution; another brand CCD camera (1024 × 768) of 358 LW/PH, about 46.6% of the limited resolution; another brand CMOS camera (3648 × 2736) of 1628 LW/PH, about 59.5% of the limited resolution. Therefore, our camera with a high precision and high spatial resolution design, it can to meet in OCT and increase accuracy of the dose distribution.

1. Introduction

Our goal is to design a highly reliable camera system (low-noise and high SNR ratio), but also has a high-resolution output, so the image sensor use CCD (Charge Coupled Device). CCD image sensor are better than the performance of CMOS (Complementary Metal Oxide Semiconductor) image sensor, because the sensor architecture, CCD output noise is lower than CMOS, so the reliability of the image is better than CMOS [1,2]; in the same size or pixel pitch, CCD is using a special manufacturing process, CMOS is integrated circuit design, so the CCD pixel size can be made bigger than CMOS, making each pixel can get greater the amount of light, with a higher sensitivity [3,4]. CCD can create an environment in poor condition have better image quality, especially in the dark with the exception of temperature and humidity conditions.

CMOS is modular design, meaning integrated CMOS sensor, sampling circuit and the ISP (Image Signal Processor), so output image is included AEC (Auto Exposure Control, automatic exposure control), AGC (Auto Gain Control,

* Corresponding author.
E-mail address: songchen@ncut.edu.tw (W.-T. Sung).

http://dx.doi.org/10.1016/j.measurement.2014.09.068
0263-2241/

AGC) and AWB (Auto White Balance, Auto White Balance) and other algorithms, Although the images through a variety of algorithms can get good quality, but lost the original signal authenticity. Because of our goal is to be applied on medicine-related topics, medical imaging requirements are very stringent, must ensure that the integrity and authenticity of the image. Therefore, this thesis aims to make a camera system with raw data output. From the sensor signal sampling, analog-to-digital signal conversion, ISP (Image System Process) design, Host-side GUI (Graphical User Interface), etc., are all aspects of own planning and design, to ensure access the original image sensor signal. The output images with low noise and high SNR (Signal to Noise Ratio, SNR), we have to complete AFE (Analogy Front End, analog front-end circuit), FPGA ISP, GUI design and CCD signal processing algorithms.

Domestic and foreign research is committed to gel dosimetry development and research, and OCT dosimeter have been increasing research attention of scholars [5], The first set of OCT-based dosimeter of Gore scholars who proposed in 1996 [6]. In addition, based on the OCT gel dosimeter can be divided into three types: first-generation laser configuration, cone-beam CCD configuration and parallel-beam CCD scanner.

The three types of OCT using CCD-based detector (camera) [7–10], shows the CCD image sensors in medical aspects importance. Which, Sampaio scholars mentioned CCD detector (Camera) used in the gel dosimetry is required on two main characteristics: high accuracy and high spatial resolution [11]; Chang scholars in the OCT development of three-dimensional imaging system using the specifications of camera resolution is 1024 × 768 CCD (8-bit) [12]. And Thomas scholars in their dosimetry studies, camera using the specifications for the 1040 × 1392 resolution of the CCD image sensor (12-bit) [13]. In addition, Thomas scholars in their gel dosimetry study pointed out that the dynamic range of the detector requires more than 60 dB [14]. Above research, we develop a high reliability camera system with high accuracy and high spatial resolution, the camera output resolution up to four megapixel (14-bit, 2336 × 1752, the dynamic range of 64 dB). For gel dosimeters can be interpreted accurately rate increase, the relative treatment plan can be more perfect.

Design of low-noise camera system, not only AFE design, but also need for the CCD signal analyzed and discussed. The CCD output signal will be change with the incident light vary. However, in the absence of CCD image sensor when the light enters, still have a slight signal output, the effect of dark current and bias clamp caused [15]. Among them, the dark current is mainly limited by the temperature and the exposure time; while bias clamp mainly by the amplifier in the signal conversion. In both noise filtering methods, the use of a cooling device will CCD work in zero temperatures below, it can greatly reduce the impact of dark current [16]; let the CCD image sensor into dark mode can be observed bias impact [17]. In addition, the image signal is sent to the back-end before the CCD signal sampling and signal amplification process will cause a reset noise, frequency noise and amplifier noise, in these three noise filter relies on CDS (Correlated Double Sampling) [18–20].

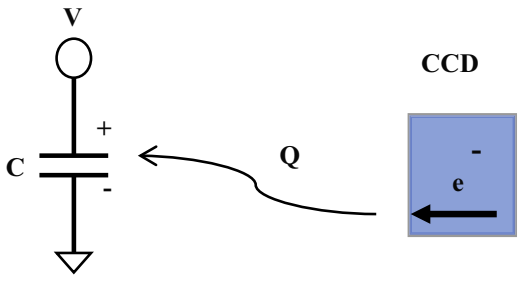

Fig. 1. Schematic of Signal Detection.

The CCD image sensor in the photoelectric conversion process, resulting in a frequency-independent white Gaussian noise [21,22], Veerakumar scholars proposed adaptive median filtering algorithm can reduce the impact of white Gaussian noise [23] , but also to the white noise, bad pixels, salt and pepper noise doing smoothing filter [24,25]. Finally, since the dark current for each pixel on the CCD inconsistency degree of influence will cause FPN (Fixed Pattern Noise) [19,26,27]; while sensing capability inconsistency between pixels is caused by PRNU (Photo Response Non Uniformity). These two are known as pattern noise, the impact of FPN is usually smaller than the PRNU, whether for CCD image sensors used in X-ray detector, both need to be PRNU correction [28,29], in which Zhu scholars have proposed the FPGA-based PRNU correction method to improve the case of non-uniformly [30], the PRNU correction can also reduced OCT imaging artifacts arising [31].

Since the majority of CCD matrices available at present are characterized by non-square point grids, many problems to be solved in image processing require square point grids in order to obtain results of invariable positions. Authors discussed that several CCD elements are used as examples to explain various methods of horizontal and vertical geometric correction intended to obtain square point grid systems [32]. Authors employed the plastic scintillation fiber (PSF) array coupled with CCD for X-ray imaging and detection. Comparing to currently available commercial computed tomography systems, since their method is relative simple, low cost, high performance, and requires a few necessary instruments, the design will find more application in radiation imaging and detection fields [33].

Authors implement a high-resolution system that investigate the use of four linear CCD image sensors, which is 2048 pixels with a size of 0.014 mm by 0.014 mm and relatively small, in an optical tomographic instrumentation system used for sizing particles. Spherical shaped and irregular shaped particles are tested on their designed system to complete analysis of the overall performance of their system [34]. Based on the stroboscopic lightning, the authors develop the vibrometer, a low cost CCD camera and a phase difference algorithm to effectively measure inplane displacements of micro-devices. A precision of 100 pm can be achieved with the measure of the vibration of an atomic force microscope cantilever [35].

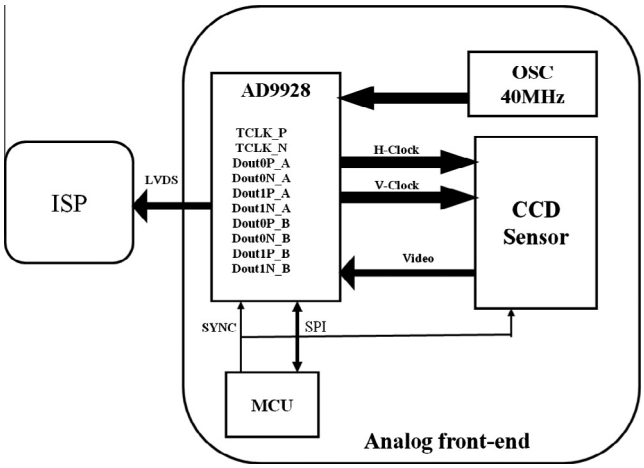

Fig. 2. AFE architecture.

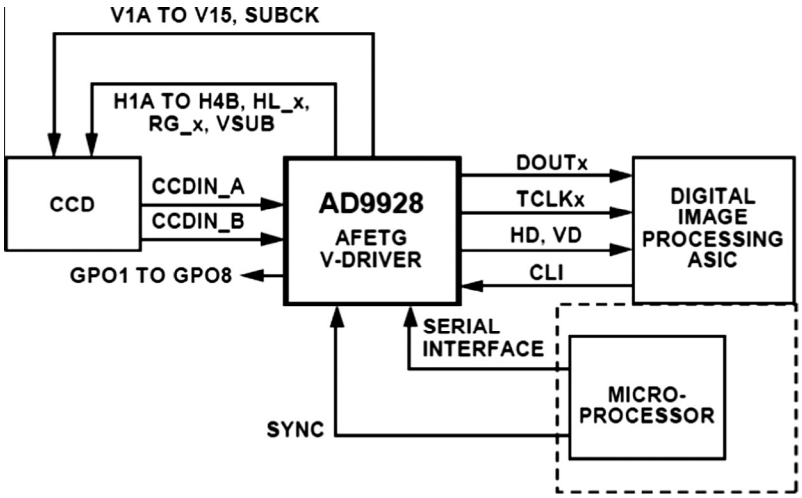

Fig. 3. AD9928 block diagram.

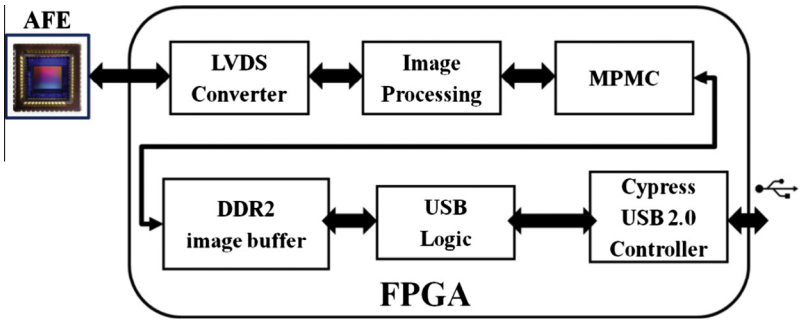

Fig. 4. ISP architecture.

Since the radiation therapy requires the precise positioning and accurate doses, a better performance can be used to improve the reliability of radiation therapy. The HD features can increase the amount of the detail shape of the contour measuring gel. The high dynamic range feature can be measured to a wider range of doses. The low noise characteristics can improve the image quality of the measurement. The sensitivity and enhancement light can improve the speed of the interception image. Therefore, one of high-resolution camera designs with

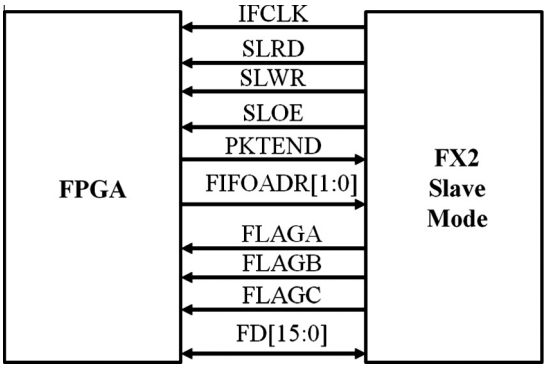

Fig. 5. FX2 slave mode.

the high dynamic range, low noise, and high sensitivity properties can be used to improve the precision of radiation position location calibration and accuracy of dose. Hence, our study will be based on these properties to design.

2. Background knowledge

2.1. Image sensor

The image sensor also known as photosensitive element, CCD sensor architecture proposed in 1969 by Bell Laboratories in the United States George Smith and Willard Boyle, With its photodiode for photographic action, then through the capacitor to store optical signal, shown in Fig. 1. After a series of signals by transfer signal sampling and signal amplification circuit to complete.

2.2. Optical lens

Optical lens selection is also important, if the image quality provided by the lens cannot be satisfied with the image sensor, it will makes the overall MTF (Modulation Transfer Function) decreased. The selection method of considering lens unit distance can be provided to the number of lines, this value can be obtained by lens manufacturer, the image sensor limit of resolution conversion method as formula (1).

$$N_f = \frac{1}{2 \times \text{pixel size}} \ (\text{cycles/mm}) \tag{1}$$

where N_f represents the resolution limit is meet at the Nyquist sampling theorem [36], the resolution of the lens must be greater than or equal to twice the spatial resolution, where pixel size is pixels in the image sensor size. We are using the image sensor pixel size of 5.5 μm, then we obtain the limit of resolution of the system is 90.91 line pairs per millimeter (lp/mm), so the lens must be selected number of pairs is greater than 90.91 lp/mm. Therefore, we selected central and peripheral of lens which providing 100 lp/mm (M1425MP).

2.3. Analogy front-end unit

Optical lens, CCD image sensor, A/D converter circuit, power circuits, etc., all belong AFE, shown in Fig. 2. First, we use the MCU (Micro Controller Unit) through SPI (Serial Peripheral Interface) to initialize the relevant action on the AD9928 registers. Then AD9928 will send the corresponding H-Clock and V-Clock signal to CCD image sensor, if CCD image sensor receives the correct drive signal, than will begin output image signals data. Finally AD9928 will convert image signals into LVDS serial signal output.

2.4. Analogy–digital signal converter

Front of the image sensor will send an analog signal, and then must be use ADC (Analog to Digital Converter) to convert analog signals to digital signals. We use the AD9928 chip, which can provide 14-bit quantitative capabilities, and LVDS signal output, architecture shown in Fig. 3 [37]. Its digital signal output includes: digital data, clk sync signal, HD, VD. Which DOUTx is 14-bit, so the data bus represents Data 0 to Data 13. And tclk is synchronous signals, providing the back-end image system processor. The horizontal sync signal HD, and VD is the vertical sync signals.

2.5. Image system processor

ISP is based on FPGA (Field Programmable Gate Array) design, it can handle high-speed video signal. We use the Digilent's Atlys Spartan-6 FPGA development board [38], this development board provides a very useful peripheral interfaces can be applied to image processing. Such as the following: VHDCI (Very High Densitycable Interconnect) interface, HDMI (High Definition Multimedia Interface) input/output interface, and USB (Universal Serial

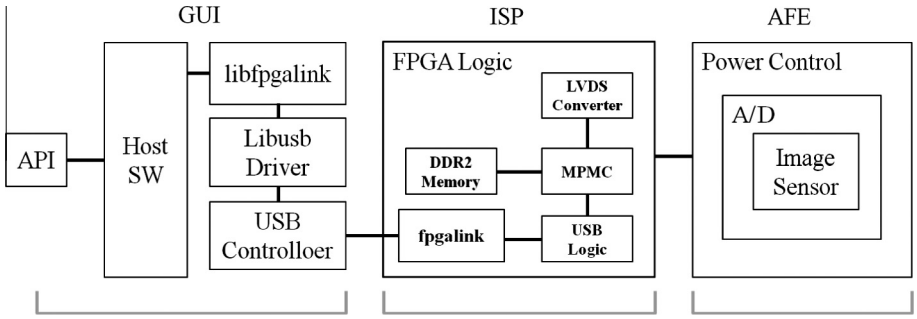

Fig. 6. Overall system architecture diagram.

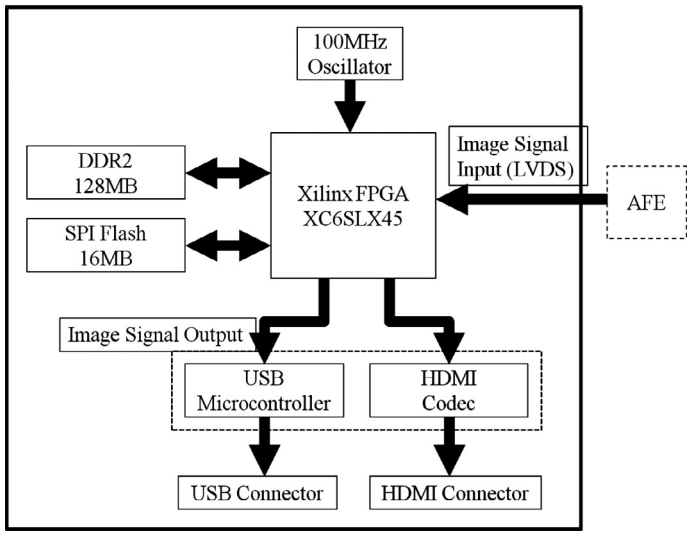

Fig. 7. ISP block diagram.

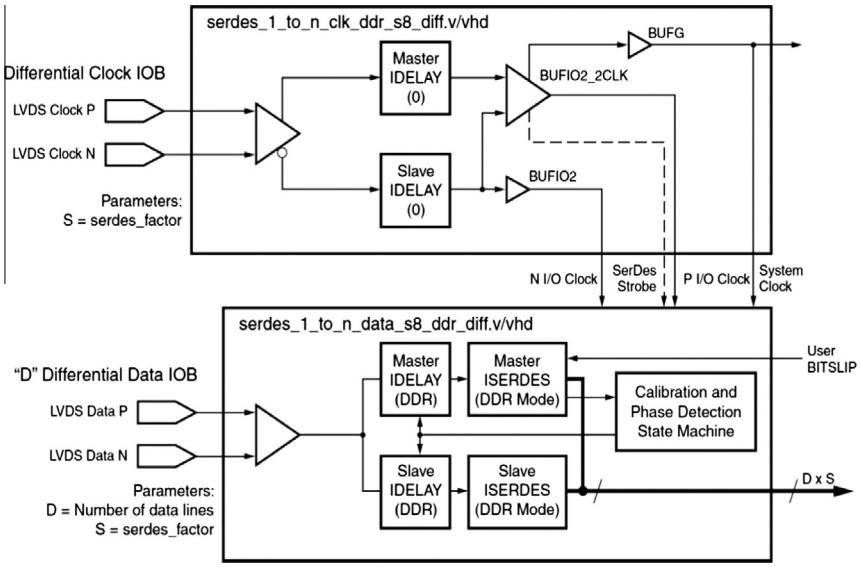

Fig. 8. Double data receiver architecture.

Bus) interface. This development board also provides a 128 Mbyte DDR2 (Double Data Rate) Memory available image data buffer to use, so it is suitable for our camera system, the overall ISP architecture shown in Fig. 4.

2.6. Image transfer mechanism

Consider the image transmission mechanism, The DVI I/F, HDMI I/F combines video capture card, which before transfer of image data must be color space conversion; While Camera Link I/F is good mechanism, but there is the high cost of hardware and universal problem. Therefore, we use the USB 2.0 protocol as a transport mechanism is very appropriate, and its theoretical transfer rate up to 480 Mb/s, coupled with low cost and easy to connect with the computer. We use the USB 2.0 controller chip: CY7C68013A-56 (FX2-LP). The USB controller provides Control, Interrupt and Bulk three transmission modes, considered the high-speed transfer of image data, so use of bulk transfer mode. while running in this mode using the Slave FIFO mode, which does not require the USB controller CPU's processing, only need to use an external endpoint (Endpoint) state can achieve high-speed transmission [39], shown in Fig. 5. Only for a few I/O can be done to control the image transfer mechanism. In the implementation we use of FPGALink [40] provided USB control logic, and FX2 firmware design, the open source project provides transmission between USB and FPGA solutions.

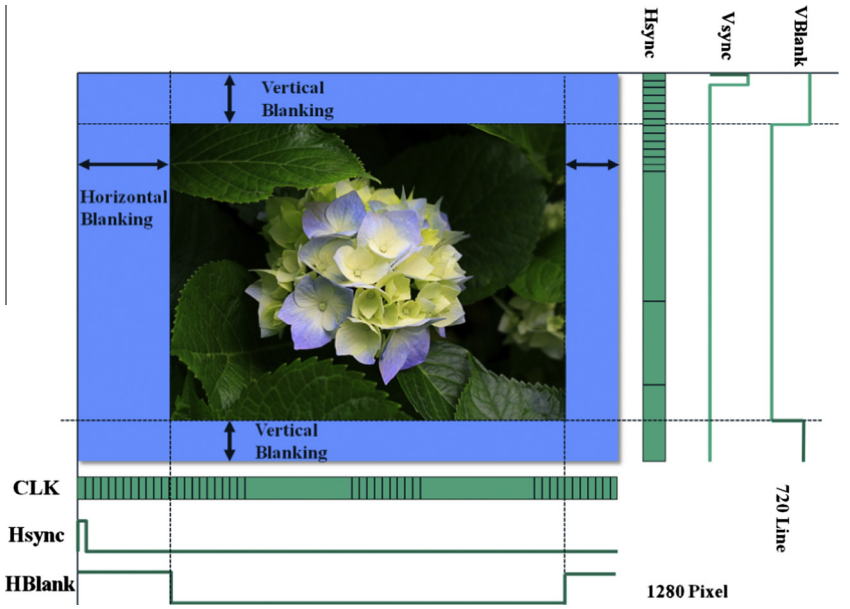

Fig. 9. Output image signal sample.

Fig. 10. Actual operational situation of camera system.

3. System architecture and design principles

3.1. System architecture

Camera system architecture shown in Fig. 6, its structure by function can be divided into three blocks, functions are described as follows:

AFE: Use high lp/mm lens, image sensor using CCD, is designed to support multiple resolutions framework, the current implementation of the maximum output resolution is 2336×1752 (4 megapixels). And use the 14-bit ADC to sampling of charge on the CCD. Finally, image data by LVDS I/F output.

ISP: ISP design based on FPGA architecture, through variety of IP's design to complete Image transfer capabilities. Firstly, use the LVDS Converter to convert differential signal into parallel signals; and then written image frame into the DRAM buffer; finally by USB Logic to complete image transfer.

GUI: Graphical User Interface programming, we use FPGALink provide solutions to complete the Host

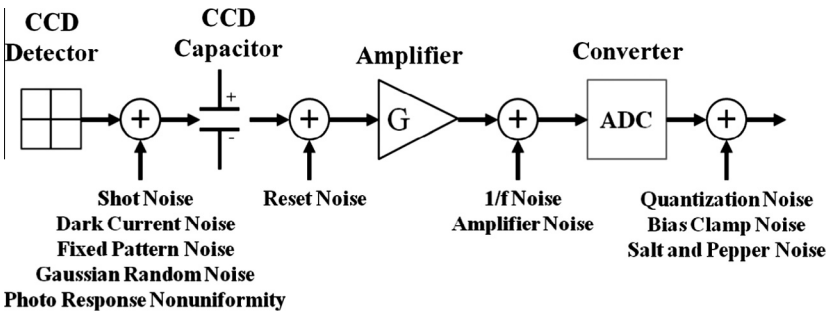

Fig. 11. CCD noise.

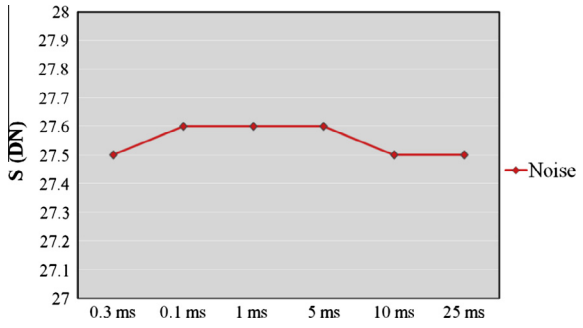

Fig. 12. Bias experiment.

architecture, when the API (Application Programming Interface) send images demand, libfpgalink communicate with libusb driver, then libusb driver send command for USB Controller, and finally resolved instructions by the ISP's USB logic to complete the overall Image transfer processes.

3.2. Image system processor module design

ISP the planned features include: LVDS converter, Image signal processing, frame buffer design and USB logic, shown in Fig. 7. The LVDS converter convert the AFE LVDS image data to digital signal (clk, hsync, vsync, raw data). And written the active image data into DDR2 memory buffer by MCB (memory control block), and finally through the USB logic to complete image read function.

3.3. LVDS converter

LVDS is low-voltage differential signal, with high speed, high noise suppression and low power consumption. In implementation, FPGA Spartan-6 chip provides SerDes (serial/deserializer) components can be used to convert the LVDS. Reference Xilinx provided XAPP1064 to complete the serial signals conversion. We use the XAPP1064 DDR data reception architecture shown in Fig. 8 [41]. We only need to set the correct parameters. The AFE LVDS output pin which TCLK_P and TCLK_N connected to LVDS clock P and LVDS clock N; while Dout0P_A, Dout0N_A, Dout1P_A and Dout1N_A connected to the LVDS Data P [1:0] and LVDS Data N [1:0]. Number of data lines is set to 2, serdes_factor set to 8.

3.4. Active frame processing

When finished LVDS conversion, the serial signals converted to parallel signals, we called raw data, The raw data is the image sensor pure signal, without any color space conversion, and raw data contains 14-bit data bus, clock signal, vsync and hsync of 17 lines. We can use these signal to accomplish active frame capture functions.

In fact, that signal does not provide the exact location of the active frame, so we use the received signal into a valid image signal, and generates the H_blank, V_blank signal, shown in Fig. 9. And H_blank, V_blank signal generation method must match the front-end CCD image sensor, the image sensor output signal not only with valid frame, but also have dark zone, dummy zone and buffer zone signal. So must doing active frame processing before storage frame data.

Table 1
Comparison quantization noise.

ADC bits	$N_{ADC(rms)}$ / $\frac{N_{Charge\ Capacity}}{2^N\sqrt{12}}$	$N_{SYS(rms)}$ / $\sqrt{N_{floor}^2+N_{ADC}^2}$
8 bit	22.55	$\sqrt{12^2+22.5^2}=25.5$
12 bit	1.41	$\sqrt{12^2+1.41^2}=12.08$
14 bit	0.35	$\sqrt{12^2+0.35^2}=12.01$

3.5. Image frame buffer design

When the image being displayed, must have a frame buffer mechanism. Based on the implementation of DDR2 memory to complete, with examples of the application provided by Xilinx XAPP496 [42]. For MCB configuration, we only need to be completion of User Logic control, and provide a variety of needed clock signal for MCB, the detailed construction method and description may refer to Xilinx provided User Guide (UG388 and UG416).

3.6. Graphical user interface design

Besides the camera system design, but also includes GUI development of the user interface to receive camera's image data. While the ISP is take USB controller to transfer image data, so the PC-side must be through the USB driver to receives image datas. The FPGALink also provides computer side solution, wherein the libfpgalink DLL provides amount of API functions, and is also complete communicate with Libusb-win32 USB driver [43]. We choose the Visual Studio [44] IDE, in order to complete the Visual C++ development tool, and use OpenCV [45] which provided image library to complete the function of a displayed image. Fig. 10 shows the actual operational situation of camera system.

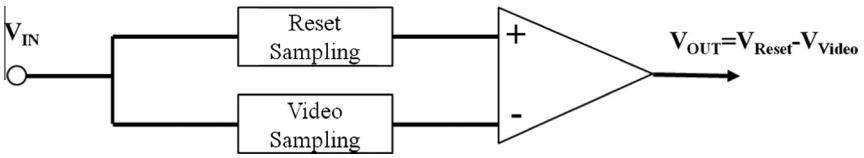

Fig. 13. Correlated double sampling circuit.

Fig. 14. Addition salt and pepper noise simulation, (a) 10% Ratio of noise. (b) After median filter.

Table 2
PSNR.

Noise ratio (%)	After median filter PSNR (dB)
1	35.40
3	35.06
5	34.78
10	33.67
15	31.76

3.7. CCD signal processing

CCD signal processing aims is elimination of noise, thus improving the overall SNR value. Fig. 11 shows the CCD exit of noise [46].

3.8. Bias noise and dark noise

The bias noise is mainly influenced by the signal conversion amplifier, called by the essential noise. The dark current is mainly limited by the effects of working temperature and exposure time. Therefore, to reduce the CCD working temperature can effectively reduce the impact caused by the dark current [16]. ADC has a bias circuit, also called as offset signal level [37]. Its purpose is to avoid the signal cannot be converted values below 0. Let CCD image sensor into dark mode, the read signal value is bias and dark current caused. We recorded the signal value of different exposure time, shown in Fig. 12.

Based on the observed results that the exposure time of the dark current affect is very small, so signal value is bias clamp. So if necessary, the direct deducting 28 value of the signal can filter bias clamp.

3.9. Reset noise, frequency noise, and amplifier noises

The reset noise, frequency noise, and amplifier noise, To reduce these three noises, the reset noise, frequency noise, and amplifier noise, we can rely on CDS (Correlated Double Sampling) circuit correlated double sampling [18,19]. Reset noise also called KTC noise, primarily due to the CCD's FD (Floating Diffusion) capacitance, and use the CDS (correlation double sampling) circuit to eliminate this noise, CDS circuit is shown in Fig. 13.

When reset, the Reset sampling circuit switch turn off, and resets signal voltage value is recorded in the capacitor

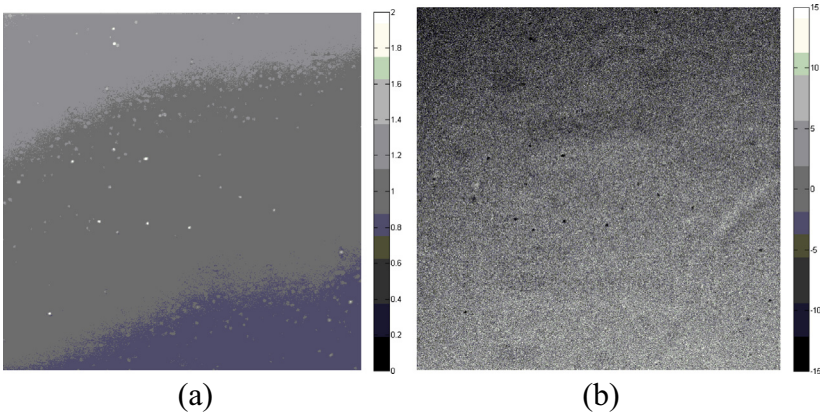

Fig. 15. Correction matrix of each pixel, (a) Slope matrix. (b) Intercept matrix.

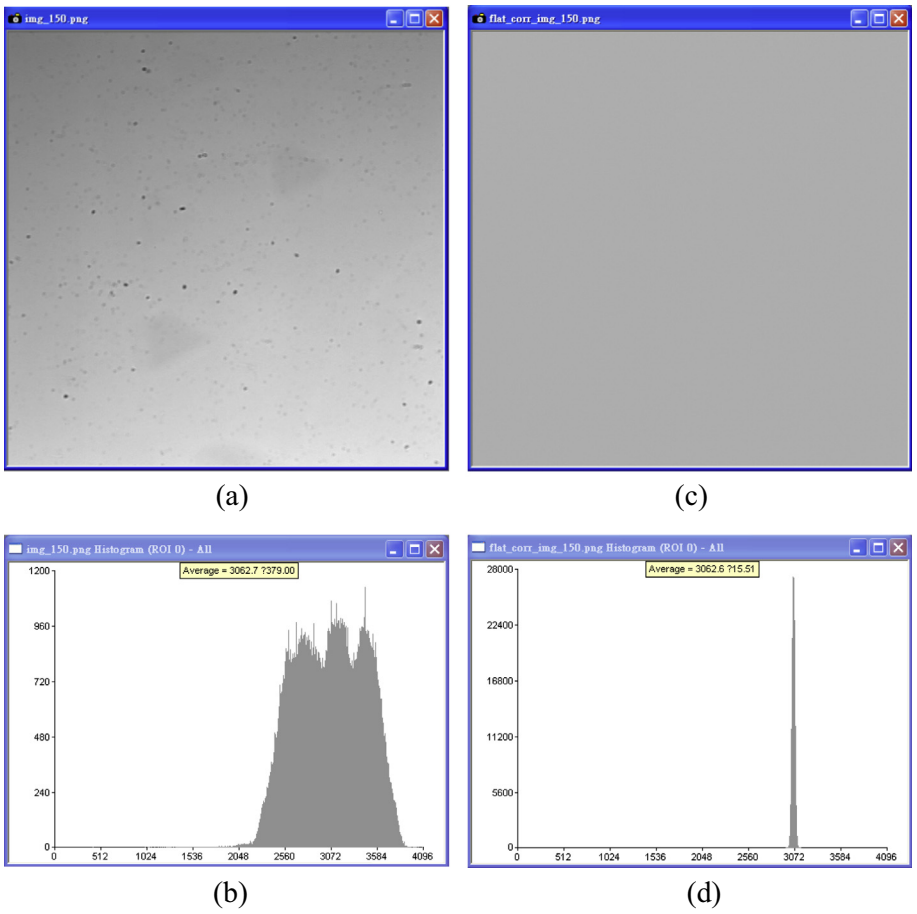

Fig. 16. Correction matrix into original image and experimental results, (a) Image at 150 ms. (b) Value before correct. (c) Image after correct. (d) Value after correct.

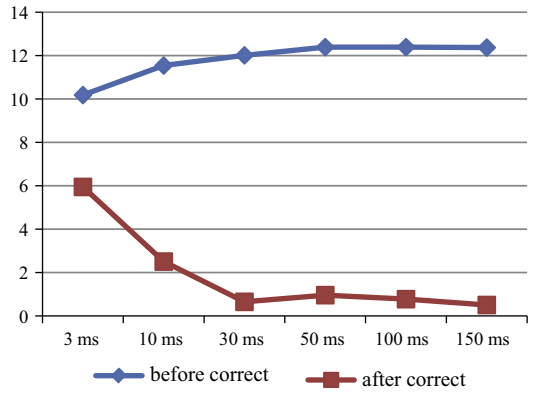

Fig. 17. Coefficient of variation before and after correction.

of sampling circuit; when Video been active, Video sampling circuit switch turn off, and value of the signal will be recorded in the capacitor of sampling circuit. Finally through the CDS circuit composed of a differential amplifier for signal subtraction operation, this way can be deducted reset noise, equivalent to $V_{OUT} = V_{IN+} - V_{IN-}$. The CDS circuit can also filter the amplifier noise and $1/f$ Noise [46,47].

3.10. Quantization noise

If choose mismatch of ADC, which will produce quantization error situations, such as those near the analog input value corresponds to the same digital output values. We list 8-bits, 12-bits and 14-bits for comparison, and charge capacity is 20,000 electrons, noise floor is 12, as shown in Table 1. Select more than 12-bit ADC can eliminate the quantization noise, so we used the 14-bit ADC can be minimized quantization noise.

3.11. Gaussian random noise, white noise, and bad pixel, and pepper noises

Veerakumar scholars proposed adaptive median filtering algorithm can reduce the impact of white Gaussian noise [23], but also to the white noise, bad pixels, salt and pepper noise doing smoothing filter [24,25]. The CCD sensor will produce the white noise, which is by the random distribution, for the working temperature rise or long exposure time [3]. The white noise can also be called temporal noise or Gaussian noise problems caused by the sensor itself. Before dealing with the pattern noise, must

Table 3
Listing of the noise type and the function for reducing noise.

Noise type	Function for reducing noise	
	Our design	Literal [20]
Bias noise	Yes	No
Reset noise, 1/*f* noise, Amplifier noise	Yes	Yes
Quantization noise	Yes	No
Gaussian random noise	Yes	No
White noise, Bad pixel, Salt & Pepper noise	Yes	Yes
FPN noise	Yes	Yes
PRNU noise	Yes	No

be dealing the random noise first. During random noise filter before using the image average way to reduce the impact of Gaussian random noise, then use the median filter algorithm to filter out noise, the method as formula (2):

$$\text{frame}_{\text{de-noise}} = \text{Med Filter}(\text{frame}_{org}, m \times n) \quad (2)$$

wherein the $m \times n$ is the mask window, we use the 3×3 window to be filtered; the algorithm compares the current pixel adjacent pixels (3×3) after removing and sort the selection of the intermediate value as the current pixel output value. It can be filter abnormal noise. We use the standard Lena picture (512×512) to verification experiments. Add salt and pepper noise simulation as random noise (white noise, thermal noise, bad pixel), and noise ratio from 1%, 3%, 5%, 10%, 15% to 20%, shows in

Table 4
the PRNU calibration results of our design.

Light output (%)	26	32	48	72	96
Before correction coefficient of variation (%)	17.22	18.64	18.86	18.89	18.71
After correction coefficient of variation (%)	0.99	0.48	0.47	0.79	0.32
Performance improvement (%)	94	97	96	95	98

Table 5
the PRNU calibration results in [49].

Light output (%)	16	32	48	72	96
Before correction coefficient of variation (%)	8.9	8.7	8.5	8.3	8.3
After correction coefficient of variation (%)	2.3	2.4	2.3	2.1	2.0
Performance improvement (%)	74	72	72	74	75

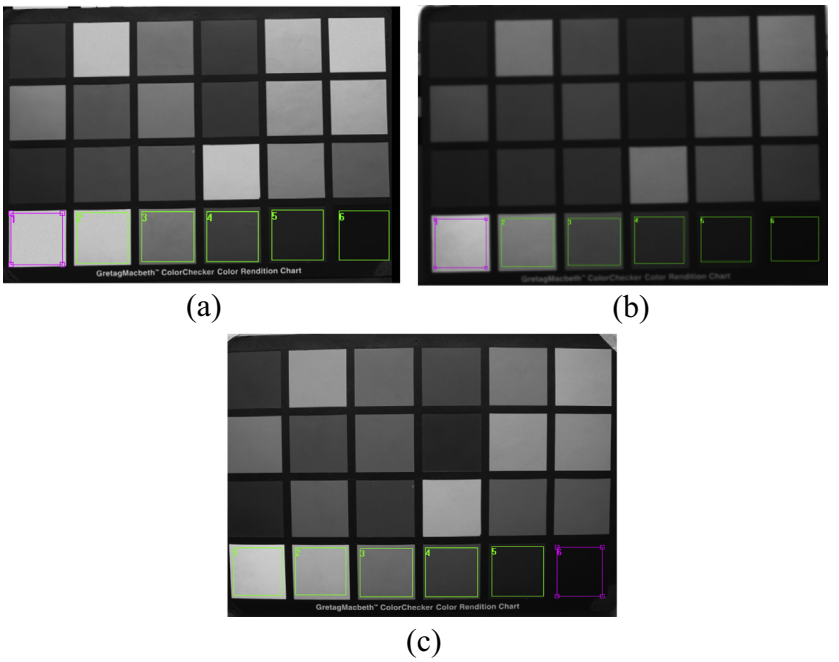

Fig. 18. Measurement SNR of Colorcheck'block No. 19 to No. 24, (a) Our camera. (b) Other CCD camera. (c) Other CMOS camera.

Table 6
Comparison of SNR.

Colorcheck chart	$= 20 \times \log_{10} \frac{\text{ROI mean}}{\text{standard deviation}}$		
	Our camera (dB)	Other brand CCD (dB)	Other brand CMOS (dB)
No. 19	35.33	25.31	29.53
No. 20	33.16	26.28	29.23
No. 21	25.90	25.99	26.42
No. 22	24.87	24.57	23.71
No. 23	24.97	23.11	19.35
No. 24	25.41	20.67	18.37

Fig. 14(a) and (b). Finally, the PSNR can be found in Table 2. In 10% noise ratio of cases are adequately noise filtering effect, while the camera system does not appear so serious noise in runtime, so the median filter is very suitable to reduce random noise method.

3.12. FPN and PRNU

FPN and PRNU noise also called pattern noise, but the pattern noise is dominated mainly by the PRNU noise. Because quantum effects, detector size, CCD image sensors bad installation, the lens around and dust obscuration effects, resulting in between each pixel sensing capability inconsistent. We use the least squares method to improve the situation of uneven pixel sensing capability [29], the linear fit to find the regression line, such as formula (3) [48]:

$$\text{linfit}_{n=1 \text{ to } N}\{\text{Pixel}_n(x,y)\} \tag{3}$$

Using six different exposure times (3 ms, 10 ms, 30 ms, 50 ms, 100 ms, and 150 ms) for linear regression, each pixel was individually correction factor (slope and intercept as shown in Fig. 15(a) and (b)).

The correction matrix into original image and experimental results are shown in Fig. 16(a–d), and the coefficient of variation before and after correction are shown in Fig. 17.

3.13. Performance comparison for the noise characteristics of technology

The 640 × 640 and 8-bit ADC as their camera specifications are discussed in [7], and the 768 × 576 and 8-bit ADC of camera specifications on their dosimetry studies [10]. Chang scholars in the OCT development of three-dimensional imaging system using the specifications of camera resolution is 1024 × 768 CCD (8-bit) [12]. And Thomas scholars in their dosimetry studies, camera using the specifications for the 1040 × 1392 resolution of the CCD image sensor (12-bit) [13]. In addition, Thomas scholars in their gel dosimetry study pointed out that the dynamic range of the detector requires more than 60 dB [14]. Above research, we develop a high reliability camera system with

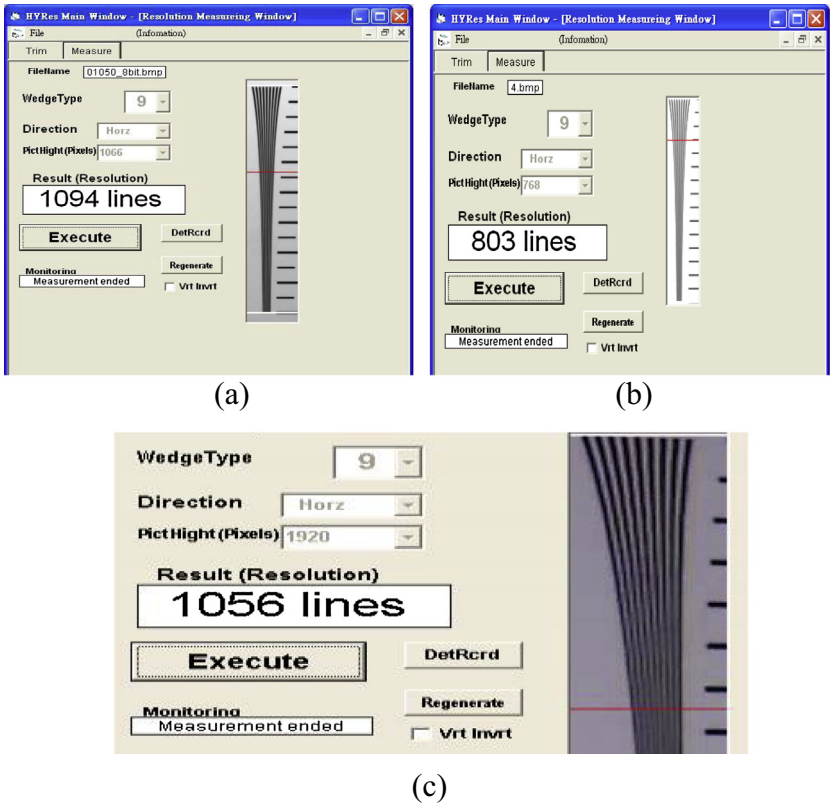

Fig. 19. TV-line measurement results, (a) Our, 1094 lines. (b) Other CCD, 803 lines. (c) 5-Megapixel IPCAM, 1056 lines [36].

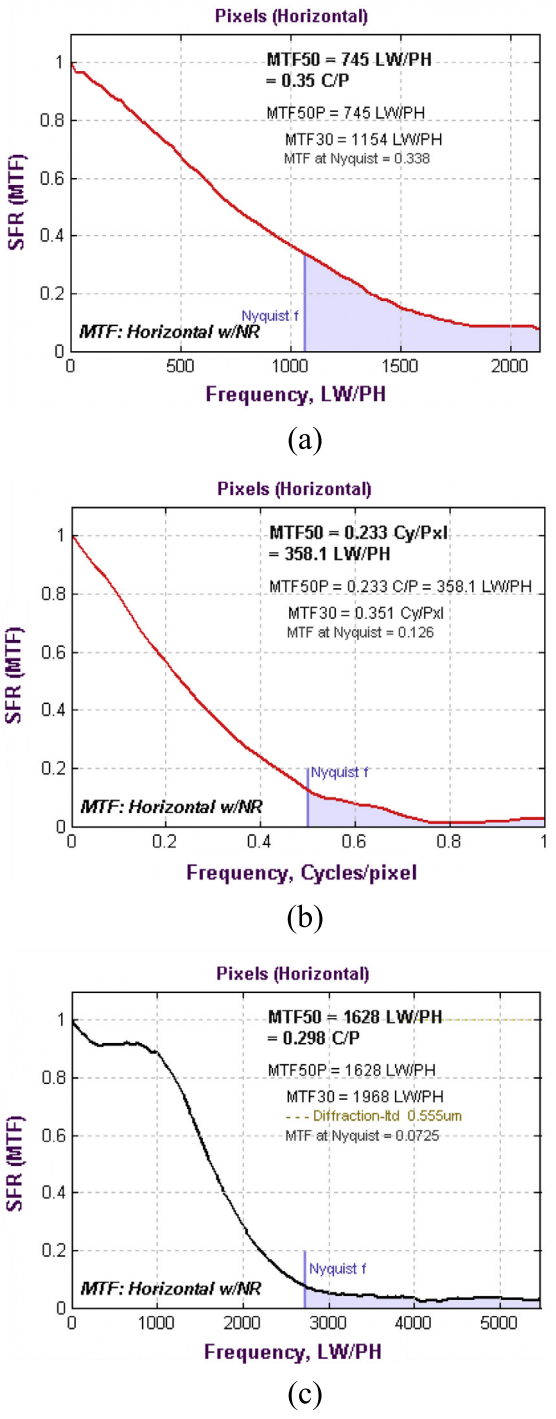

Fig. 20. SFR measurement results, (a) Our CCD: 745 LW/PH, 0.35 C/P. (b) Other CCD: 358 LW/PH, 0.233 C/P. (c) Other CMOS: 1628 LW/PH, 0.298 C/P.

high accuracy and high spatial resolution, the camera output resolution up to four megapixel (14-bit, 2336 × 1752, the dynamic range of 64 dB). For gel dosimeters can be interpreted accurately rate increase, the relative treatment plan can be more perfect.

Design of low-noise camera system, not only AFE design, but also need for the CCD signal analyzed and discussed. The CCD output signal will be change with the incident light vary. However, in the absence of CCD image sensor when the light enters, still have a slight signal output, the effect of dark current and bias clamp caused [15]. Among them, the dark current is mainly limited by the temperature and the exposure time; while bias clamp mainly by the amplifier in the signal conversion. In both noise filtering methods, the use of a cooling device will CCD work in zero temperatures below, it can greatly reduce the impact of dark current [16]; let the CCD image sensor into dark mode can be observed bias impact [17]. In addition, the image signal is sent to the back-end before the CCD signal sampling and signal amplification process will cause a reset noise, frequency noise and amplifier noise, in these three noise filter relies on CDS (Correlated Double Sampling) [18–20]. Comparison performance of the listing of the noise types, the bias noise, reset noise, $1/f$ noise, amplifier noise, quantization noise, Gaussian random noise, white noise, bad pixel, Salt & Pepper noise, FPN noise, and PRNU noise [20], and their corresponding functions for reducing noise are shown in Table 3. All of their corresponding functions for reducing noise can be enable in our study and only partial corresponding functions can be enable in the other design one as shown in Table 3.

About the PRNU performance of the pixel sensor, the calibration performance of our design is shown in Table 4 and the other design is shown in Table 5, respectively. The PRNU calibration performance of our design is based on the PC and the other design is based on FPGA. Since the image noise after the correction coefficient of variation of our design can greatly decrease the influence caused by PRNU as shown in Tables 4 and 5, we can see that the correction method used in this study had better calibration results than that of [49]. Hence, compared the PRNU performance with the literature, the results in Tables 4 and 5 indicate that our design can get the better performance than that of the literal [49].

4. Experiments and measurements

4.1. Noise measurement

Use the Colorcheck'block No. 19 to No. 24 to measure the SNR of each block as shown in Fig. 18(a–c), the conversion formula as shown in Table 6.

4.2. TV-line measurement

Resolving power, also called spatial resolution, which is defined as LW/PH (Line Width/Picture Height). Resolving power influenced by the following factors: the lens, image sensor, AFE, ISP and image compression. We use the Olympus company provides measurement software [50], the measurement results shown in Fig. 19(a–c). Which Fig. 19(a) as a measurement result of our CCD camera (1024 × 1024); Fig. 19(b) as a measurement result of other brand CCD camera measurement (1024 × 768); Fig. 19(c)

as a measurement result of 5-megapixel IPCAM (Internet Protocol Camera).

4.3. SFR measurement

SFR (Spatial Frequency Response) is similar to MTF (Modulation Transfer Function), the concept of a transfer curve function to describe the camera's sharpness ability [51], using Imatest Software measurement [52].

The measurement results are shown in Fig. 20(a–c). Three different cameras from the measurement results, the measurement results of our camera was 745 LW/PH and 0.35 C/P (Cycle/Pixel); the other brand CCD camera was 358.1 LW/PH and 0.233 C/P; the other brand CMOS camera was 1628 LW/PH and 0.298 C/P. The first values is how much number of pairs can display in fixed picture height, while the second value C/P is each pixel to express how much the number of cycle. The other brand CMOS camera is 10-megapixel level, so the LW/PH value is higher than our camera; but in the C/P value is less than our camera. As a result, our camera in the spatial resolution are better than 10-megapixel grade's camera.

5. Conclusion

We propose a high accuracy and high spatial resolution camera system, through our AFE module, ISP module and GUI design, via the USB interface to transfer image raw data. So we can directly use raw data to processing signal noise, and further complete a variety of noise filter. The experimental results, bias and dark current caused by the effect of approximately 28 S(DN); the median filter can eliminate the gaussian white noise, white noise and salt and pepper noise. As for the FPN and PRNU noise after flat-field correction algorithms, it can drop the standard deviation of the image, when exposure time at 150 ms, the image of the coefficient of variation decreased from 12.37% to 0.51%. In same measurement standards, the SNR in the best case our camera (35.33 dB) better than other brand CCD camera (25.31 dB) and other brand CMOS camera (29.53 dB). In MTF50 conditions, our camera at 1024×1024 resolution, the output was 745 LW/PH, equal to 73% of the limit resolution; other brand CCD camera (1024×768) was 358 LW/PH, about 46.6% of the limit resolution; while other brand CMOS camera (3648×2736) was 1628 LW/PH, about 59% of the limit of resolution. Also in the TVL measurement results of our system (1094 lines) is also greater than other brand CCD camera (803 lines) and other brand 5-megapixel IPCAM (1056 lines).

As a result, our camera is a high precision and high spatial resolution design, not only can meet in Optical-CT scanner application. But also can applied to different application, such as security surveillance market, machine vision, and coastal areas science and technology. And part of future work, the camera system implementation uses the USB 2.0 to complete the image transfer function. As USB 3.0 technology matures, the future can be considered to implement the USB 3.0, so OCT imaging time can be shortened.

Acknowledgement

This study was financially supported by the National Science Council of Taiwan (NSC 102-2221-E-159-006- and MOST 103-2221-E-159-005-).

References

[1] A. Luštica, CCD and CMOS image sensors in new HD cameras, in: The 53rd International Symposium ELMAR-2011, 2011, pp. 113–116.
[2] B. Luo, L. Yan, F. Yang, Research of noise suppression for CMOS image sensor, in: 2010 International Conference on Measuring Technology and Mechatronics Automation (ICMTMA2010), 2010, pp. 1100–1103.
[3] G. Köklü, et al., Quantitative comparison of commercial CCD and custom-designed CMOS camera for biological applications, in: The International Symposium on Circuits and Systems (ISCAS2011), 2011, pp. 2063–2066.
[4] I. Djité et al., Theoretical models of modulation transfer function, quantum efficiency, and crosstalk for CCD and CMOS image sensors, IEEE Trans. Electron Dev. 59 (3) (2012) 729–737.
[5] M. Oldham, J.H. Shetty, A. Shetty, D.A. Jaffray, High resolution gel-dosimetry by optical-CT and MR scanning, Med. phys. 28 (2001) 1436–1445.
[6] S.J. Doran, The history and principles of optical computed tomography for scanning 3-D radiation dosimeters: 2008 update, J. Phys.: Conf. Ser. 164 (1) (2009) 012020.
[7] A.E. Papadakis, et al., Development of a new laser-line and CCD based optical-CT scanner for the readout of 3D radiation dosimeters, in: IC3DDose: The 6th International Conference on 3D Radiation Dosimetry, vol. 250(1), 2010, pp. 1–3.
[8] A.E. Papadakis et al., A new optical-CT apparatus for 3-D radiotherapy dosimetry: is free space scanning feasible?, IEEE Trans Med. Imag. 29 (5) (2010) 1204–1212.
[9] A.E. Papadakis et al., Technical note: a fast laser-based optical-CT scanner for three-dimensional radiation dosimetry, Med. Phys. 38 (2011) 830–835.
[10] K. Nikola, S.J. Doran, Focusing optics of a parallel beam CCD optical tomography apparatus for 3D radiation gel dosimetry, Phys. Med. Biol. 51 (8) (2006) 2055–2075.
[11] F.G.A. Sampaio et al., Quality assurance of a two-dimensional CCD detector system applied in dosimetry, IEEE Trans. Nucl. Sci. 60 (2013) 810–816.
[12] Y.J. Chang et al., Development of a CCD-based optical computed tomography scanner used in 3D gel dosimetry, Appl. Mech. Mater. 300 (2013) 1632–1635.
[13] A. Thomas, J. Newton, M. Oldham, A method to correct for stray light in telecentric optical-CT imaging of radiochromic dosimeters, Phys. Med. Biol. 56 (14) (2011) 4433–4451.
[14] A. Thomas, J. Newton, J. Adamovics, M. Oldhama, Commissioning and benchmarking a 3D dosimetry system for clinical use, Med. Phys. 38 (2011) 4846–4857.
[15] H.C. Burger, B. Scholkopf, S. Harmeling, Removing noise from astronomical images using a pixel-specific noise model, in: 2011 IEEE International Conference on Computational Photography (ICCP), 2100, pp. 1–8.
[16] D. Zheng, J. Gong, X. Song, M. Guan, Low Noise CCD System Design and Implementation Based on Thermoelectric Refrigerating Unit, in: 2010 IEEE First International Conference on Pervasive Computing Signal Processing and Applications (PCSPA), 2010, pp. 406–409.
[17] C. Pan, et al., OMPS early orbit dark and bias evaluation and calibration, in: 2012 IEEE International Geoscience and Remote Sensing Symposium (IGARSS2012), 2012, pp. 1092–1095.
[18] R. Liu, J. Lu, J. Ding, Y. Liu, CCD Signal Processing Based on Correlated Double Sampling, in: 2011 IEEE 5th International Conference on Bioinformatics and Biomedical Engineering (iCBBE2011), 2011, pp. 1–3.
[19] M. Perenzoni et al., A 160×120-pixels range camera with in-pixel correlated double sampling and fixed-pattern noise correction, IEEE J. Solid-State Circ. 46 (7) (2011) 1672–1681.
[20] L.P. Zhang, J.Q. He, H.L. Dai, C.M. Wan, Noise processing technology of a TDICCD sensor, in: 2010 IEEE International Conference on, Computer, Mechatronics, Control and Electronic Engineering (CMCE), vol. 5, 2010, pp. 395–398.
[21] A. Jezierska, E. Chouzenoux, J.C. Pesquet, H. Talbot, A primal-dual proximal splitting approach for restoring data corrupted with Poisson–Gaussian noise, 2012 IEEE International Conference on

Acoustics, Speech and Signal Processing (ICASSP), 2012, pp. 1085–1088.
[22] A. Komaee, Nonlinear filters for bayesian estimation of pulse arrival time in additive white gaussian noise, IEEE Trans. Signal Process. 59 (10) (2011) 4850–4859.
[23] T. Veerakumar, S. Esakkirajan, I. Vennila, An efficient approach to remove random valued impulse noise in images, in: 2012 IEEE International Conference on Recent Trends Information Technology (ICRTIT), 2012, pp. 49–53.
[24] T. Veerakumar, S. Esakkirajan, I. Vennila, Salt and pepper noise removal in video using adaptive decision based median filter, in: 2011 IEEE International Conference on Multimedia, Signal Processing and Communication Technologies (IMPACT), 2011, pp. 87–90.
[25] S. Esakkirajan, T. Veerakumar, A.N. Subramanyam, C.H. PremChand, Removal of high density salt and pepper noise through modified decision based unsymmetric trimmed median filter, IEEE Signal Process. Lett. 18 (5) (2011) 287–290.
[26] M. Shahram, N.S. Mehdi, R. Sobhan, R. Saeed, A novel fixed pattern noise reduction technique in image sensors for satellite applications, Electr. Electron. Eng. 2 (5) (2012) 271–276.
[27] X.Y. Li, Z. Qu, J. Huang, Enhancing source camera identification performance with a camera reference phase sensor pattern noise, IEEE Trans. Inform. Forensics Secur. 7 (2) (2012) 393–402.
[28] Y. Yu, J. Wang, Beam hardening-respecting flat field correction of digital X-ray detectors, in: 2012 IEEE International Conference on Image Processing (ICIP2012), 2012, pp. 2085–2088.
[29] A.L.C. Kwan, J.A. Seibert, J.M. Boone, An improved method for flat-field correction of flat panel x-ray detector, Med. phys. 33 (2) (2006) 391–394.
[30] H. Zhu, et al., Correction of the non-uniformity for multi-TDICCD mosaic camera on FPGA, in: 2010 IEEE International Conference on E-Product E-Service and E-Entertainment (ICEEE), 2010, pp. 1–4.
[31] Z. Wei, S. Wiebe, D. Chapman, Ring artifacts removal from synchrotron CT image slices, J. Instrument. 8 (6) (2013) C06006.
[32] M. Idroas et al., Design and development of a CCD based optical tomography measuring system for particle sizing identification, Measurement 44 (10) (2011) 2205–2216.
[33] S. Tang, J. Xie, Q. Ma, Plastic scintillation fiber array coupling CCD for X-ray imaging and detection, Measurement 42 (6) (2009) 933–936.
[34] I.G. Heuer, Geometric correction of CCD matrices, Measurement 5 (4) (1987) 185–188.
[35] D. Teyssieux, S. Euphrasie, B. Cretin, MEMS in-plane motion/vibration measurement system based CCD camera, Measurement 44 (10) (2011) 2205–2216.
[36] H. Nyquist, Certain topics in telegraph transmission theory, Am. Inst. Electr. Eng. 47 (2) (1928) 617–644.
[37] Analog Devices Inc., AD9928 Specification, <http://www.analog.com/static/imported-files/ data_sheets/AD9928.pdf>.
[38] Digilent Inc., Atlys™ Spartan-6 FPGA Development Board, <http://www.digilentinc.com/Data/Products/ATLYS/Atlys_rm.pdf>.
[39] J.H. Park, D.R. Lee, D.K. Kim, J.W. Jeon, Implementation of a stand-alone color image transfer circuit using the USB 2.0 interface, in: International Conference on Control, Automation and Systems (ICCAS'07), 2007, pp. 2323–2328.
[40] C. McClelland, Makestuff-FPGALink, <http://www.makestuff.eu/wordpress/software/fpgalink/>.
[41] Xilinx Inc., XAPP 1064, <http://www.xilinx.com/support/documentation/application_notes/xapp1064.zip>.
[42] Xilinx Inc., XAPP 496, <http://www.xilinx.com/support/documentation/application_notes/xapp496.pdf>.
[43] P. Stuge, libusb-win32, <http://www.libusb.org/>.
[44] Microsoft Inc., Visual Studio 2010, <http://www.microsoft.com/visualstudio/zh-tw>.
[45] Open Source Computer Vision Library, <http://www.opencv.org/>.
[46] G.C. Holst, CCD Arrays, Cameras, and Displays, SPIE Optical Engineering Press, Bellingham, 1998.
[47] B. Stephan, CCD Imaging Systems, Brown Corporation, USA, 2004.
[48] J.A. Seibert, J.M. Boone, K.K. Lindfors, Flat-field correction technique for digital detectors, Medical Imaging, 98, Int. Soc. Opt. Photon. (1988) 348–354.
[49] ACTi Inc., TVL – the true measurement of video quality, <http://www.acti.com/download_file/KnowledgeBase_UploadFile/TVL-The_True_Measurement_of_Video_Quality_20101027_002.pdf>.
[50] CIPA Inc., Olympus HYRes3.1 software, <http:// www.cipa.jp/dcs/hyres/hyres_1_e.html>.
[51] C. Fan, Y.T. Liang, H.L. Fu, T.J. Yang, Research on the test target of MTF for the remote sensing camera, in: 2010 IEEE International Conference on, Environmental Science and Information Application Technology (ESIAT), vol. 1, 2010, pp. 234–236.
[52] Imatest Inc., Imatest Studio Edition software, <http://www.imatest.com>.